Sachiko Hayashi

Puf3p facilitates fermentative mitochondrial functions via monosome-enriched nuclear-encoded mitochondrial mRNAs in budding yeast

Sachiko Hayashi[1]*, Kazumi Iwamoto[2], Tohru Yoshihisa[1]

[1]Graduate School of Science, University of Hyogo, Ako-gun, 678-1297, Japan

[2]Graduate School of Life Science, University of Hyogo

* To whom correspondence should be addressed. Tel: +81-791-58-0174; Fax: +81-791-58-0180; E-mail: shayashi@sci.u-hyogo.ac.jp

Running title: Regulations of nuclear-encoded mitochondrial mRNAs via Puf3p under the fermentation

Key words: Puf3p, yeast, nuclear-encoded mitochondrial mRNAs, translation

Sachiko Hayashi

ABSTRACT

Yeasts generally grow with a highly glycolytic metabolism and restrain mitochondrial biogenesis except for some Fe/S proteins. Respiratory mitochondrial functions and biosynthesis pathways are well studied, however how cells coordinate basal fermentative mitochondrial functions is not fully understood. We show that a part of nuclear-encoded mitochondrial mRNAs, which preferentially translated in monosomes, are regulated by Puf3p upon glucose-rich media. Especially, of those monosome-enriched nuclear-encoded mitochondrial mRNAs, *CAT5/COQ7* mRNA has a variant of the canonical Puf3p binding site on its 3'-UTR. Western blot analysis showed that Puf3p represses the translation of Cat5p regardless of fermentable or respiratory media. *In vitro* binding assay revealed that Puf3p directly binds to *CAT5* mRNA via the non-canonical Puf3p binding site. Mutants harboring the substitution of the non-canonical Puf3p binding site in *CAT5* mRNA grew normally but impaired Cat5p expressions apparently, indicating *CAT5* mRNA is a bona fide Puf3p target. Overall, Puf3p, a general key modulator for nuclear-encoded mitochondrial mRNAs, fine-tunes translation of a subset of nuclear-encoded mitochondrial mRNAs including mRNAs with non-canonical Puf3p binding sites under the fermentation. This may be required to keeping the fundamental functions of yeast mitochondria at proper levels.

INTRODUCTION

Mitochondria play crucial roles for numerous cellular processes, including biosynthesis of heme and Fe/S clusters, metabolism of amino acids and lipids, and production of the bulk of ATP in many eukaryotes (Attardi and Schatz 1988; Lill and Mühlenhoff 2008; Malina et al. 2018). *Saccharomyces cerevisiae*, a classical model organism on mitochondrial research, generally prefers fermentation rather than respiration. The fermentation process using glucose is catalytically more efficient than the respiration regarding ATP production per protein mass (Nilsson and Nielsen 2016), whereas the respiration generates 10 times more ATP per glucose molecule (van Dijken et al. 2000). Only if glucose is exhausted, yeasts switch to aerobic respiration accompanying with dynamic upregulation of mitochondrial biogenesis, as the diauxic shift. Although yeasts can survive with defects in oxidative phosphorylation with complete loss of mtDNA, the mitochondrial dysfunction of Fe/S assembly is lethal (Gancedo 1998; Lill and Mühlenhoff 2008; Malina et al. 2018). Mitochondrial iron-sulfur cluster (ISC) assembly machinery is required for biogenesis of all cellular Fe/S proteins including cytosolic and nuclear Fe/S proteins that involved in DNA maintenance or protein translation. The inactive state of these cytosolic and nucleus Fe/S proteins impairs cell viability (Lill and Mühlenhoff 2008; Sharma et al. 2010).

In *Saccharomyces cerevisiae*, only eight mitochondrial proteins are encoded by the mitochondrial genome. More than 99% of all the remaining mitochondrial proteins are encoded by the nuclear genome, and translated in cytosolic ribosomes as their precursor form (Endo et al. 2011; Priesnitz and Becker 2018; Wiedemann and Pfanner 2017). Thus, correct sorting of mitochondrial proteins is the first step to ensure organellar functionality. A classical targeting pathway for mitochondrial proteins uses mitochondrial targeting sequences (MTS) mainly located on their N-terminus (Chacinska et al. 2009; Wiedemann and Pfanner 2017), whereas approximately one-half of mRNAs for nuclear-encoded mitochondrial proteins (nc-mitochondrial mRNAs) are transported to the mitochondrial surface, and translated locally (Garcia et al. 2007; Marc et al. 2002; Lesnik et

al. 2015; Sylvestre et al. 2003). Proximity-specific ribosome profiling targeting the tagged ribosomes on the mitochondrial surface showed highly enrichment of nc-mitochondrial mRNAs, especially those encoding proteins in the mitochondrial inner membrane (Williams et al. 2014). Electron cryotomography (CryoET) revealed active cytosolic ribosomes attach to the mitochondrial outer membrane and interact with the TOM complex (Gold et al. 2017). The cytosolic translation of nc-mitochondrial mRNAs and mitochondria closely interact with each other. In fact, aberrant accumulation of mitochondrial precursors in the cytosol causes mitochondrial precursor over-accumulation stress (mPOS) (Wang and Chen 2015). Alternatively, mitochondrial dysfunction triggers a cytosolic proteostasis system (Andréasson et al. 2019).

A member of the Pumilio-homology domain family, Puf3p is a well-known regulator for nc-mitochondrial mRNAs (Walters and Parker 2014; Quenault et al. 2011; Crawford and Pavitt 2019). Global analysis showed that Puf3p physically associates with 220 transcripts at least, and more than 70% of which are nc-mitochondrial mRNAs (Gerber et al. 2004). The following multi-omics analyses consistently showed binding specificity of Puf3p to nc-mitochondrial mRNAs (Hogan et al. 2008; Freeberg et al. 2013; Kershaw et al. 2015), while PAR-clip (Freeberg et al. 2013) and RIP-seq (Kershaw et al. 2015) additionally identified numerous non-mitochondrial mRNAs as Puf3p targets. Therefore, Puf3p is not a specialized regulator of nc-mitochondrial mRNAs, rather globally modulates gene expression related to mitochondrial functions.

The *puf3Δ* yeast grows slowly in the respiratory media (Gerber et al. 2004; Lee and Tu 2015), and impairs mitochondrial motility and biogenesis (García-Rodríguez et al. 2007; Lee and Tu 2015). Loss of Puf3p changes cellular oxidative stress tolerance and the glutathione redox state (Rowe et al. 2014), as well as increasing cellular oxygen consumption in a growth-dependent manner (Chatenay-Lapointe and Shadel 2011). In parallel, multiple studies reported that Puf3p destabilizes its target mRNAs by promoting deadenylation, and regulates negatively mitochondrial biogenesis under the fermentation (Chatenay-Lapointe and Shadel 2011; Foat et al. 2005; Gerber et al. 2004; Gupta et al. 2014; Jackson et al. 2004; Lee et al. 2010; Miller et al. 2014; Olivas and

Parker 2000). In agree with the repressive roles of Puf3p in the glucose-rich media, Puf3p abundance drastically reduces during the diauxic shift (García-Rodríguez et al. 2007), but meanwhile Puf3p associates with actively translating polysomes upon glucose depletion and promotes mitochondrial biogenesis (Lee and Tu 2015; Wang et al. 2019). This bi-directional functions of Puf3p are regulated by phosphorylation via casein kinase Hrr25p (Bhondeley and Liu 2020; Lee and Tu 2015). The corresponding *PUF3*(24A) mutations acts dominant negatively, and even more strongly inhibit cell growth upon the diauxic shift than the complete deletion of *PUF3* (Lee and Tu 2015), meaning that the improper phosphorylation status of Puf3p highly impacts on cellular homeostats.

Puf3p possess an eight-Puf repeats each of which comprises three α-helices, and the helices of neighboring repeats are stacked to form a crescent shape (Edwards et al. 2001; Wang et al. 2001; Zhu et al. 2009). X-ray crystallography revealed three amino acid residues within each Puf repeat directly contact with a single base of RNA and determine binding specificity dominantly (Cheong and Hall 2006; Koh et al. 2009; Miller et al. 2008; Opperman et al. 2005; Varshney et al. 1991; Wang et al. 2009; Zhu et al. 2009). The Puf3p repeat domain (Puf3-RD) is sufficient to modulate mRNA metabolism and physically interacts with target mRNAs, shown by yeast Puf3p, which binds to the 3'-UTR of *COX17* mRNA (Houshmandi and Olivas 2005; Jackson et al. 2004). Regarding the Puf3p binding motif on target mRNAs, an 8-nt UGUANAUA was identified as the consensus Puf3p binding sequence (Olivas and Parker 2000; Gerber et al. 2004; Riordan et al. 2011). PUF proteins generally bind to a typical 8-nt sequence possessing UGU(A/G) at the 5' end and more variable 3' sequences specific to the individual Puf proteins (Bernstein et al. 2005; Gerber et al. 2004; Opperman et al. 2005; Wickens et al. 2002). At least in yeast, a cytosine at the second position minus the Puf3p binding sequence was involved in Puf3p-RNA binding *in vitro* as well as biological activity *in vivo* (Zhu et al. 2009).

Mitochondrial studies uncovered the respiratory mitochondrial functions as well as cytosolic regulations regarding mRNA stability and translational control of nc-mitochondrial mRNAs.

However, how budding yeasts coordinate the basal mitochondrial functions under the fermentation are still not completely clear. Since most of nc-mitochondrial mRNAs are generally rapidly degraded and/or translationally repressed under the fermentation (Miller et al. 2014; Foat et al. 2005), we focused on monosome-enriched mRNAs identified by ribosome profiling in Heyer and Moore (Heyer and Moore 2016). These monosome-enriched mRNAs include a subset of nc-mitochondrial mRNAs, which harboring the Puf3p binding sequence as the canonical Puf3p targets. Although *CAT5/COQ7* mRNA was a non-canonical Puf3p target, our biochemical analyses clearly showed that Puf3p controls *CAT5* mRNA translation and directly binds to the *CAT5* 3'-UTR via a non-canonical Puf3p binding sequence, which possesses a nucleotide substitution at the 7th position not usually observed in the canonical one. Thus, our data certainly provide different lines of evidence regarding Puf3p functions during the fermentation, as well as pointing out wider acceptance of mRNA recognition by Puf3p.

RESULTS AND DISCUSSIONS

Categorized monosome-enriched nc-mitochondrial mRNAs show a correlation with mRNA localization on the mitochondrial membrane including Puf3p targets.

To explore the translational status of nc-mitochondrial mRNAs under the fermentable conditions, we referred to Heyer and Moore (2016), which identified monosome-enriched mRNAs in *S. cerevisiae* via ribosome profiling. The mRNAs engaging with monosome and longer than 590 nt, mainly include mRNAs for nuclear proteins, while mRNAs for mitochondrial proteins are also included noticeably (Supplemental Figure S1A). We analyzed their published dataset (NCBI's GEO: GSE76117) regarding the monosome-enriched nc-mitochondrial mRNAs more individually, and found that 75% (18 out of 24) of those mRNAs are localized on the mitochondrial outer membrane and a half of which possess the binding site for Puf3p (Saint-Georges et al. 2008; Supplemental Table S1). Puf3p, one of the Pumilio homologues, controls the translation of numerous nc-mitochondrial mRNAs via its target sequences until the mRNAs are at the vicinity of mitochondria (Crawford and Pavitt 2019; Quenault et al. 2011; Walters and Parker 2014). We speculated the monosome-enriched nc-mitochondrial mRNAs, especially those interacted with Puf3p, may reflect the intermediate status during degradation or the temporary translation-repressed status during mRNAs transport to mitochondria. According to their ribosome footprints of mRNAs in the monosome fraction, the nc-mitochondrial mRNAs regardless of whether categorized as polysome-enriched or monosome-enriched ones, have mainly a high peak of ribosome occupancy at the 5'-end of the ORFs, probably due to stalling ribosomes at the region encoding MTSs. In contrast, the polysome-enriched non-mitochondrial mRNAs possessed rather distributed monosome peaks throughout their ORF (Supplemental Figure S1B). Thus, it is likely that the nc-mitochondrial mRNAs in the monosome fraction are rather not degraded but in stand-by and/or ongoing modes for translation near the mitochondria.

A subset of nc-mitochondrial mRNAs was occupied by small numbers of ribosomes under the fermentation.

To probe further if monosome-enriched nc-mitochondrial mRNAs possess any distinctive features on their translation under the fermentable conditions, we performed the polysome analysis of wild-type and *puf3Δ* yeasts, followed by northern blotting using fractionated RNAs. Consistent with the previous report (Kershaw et al. 2015; Rowe et al. 2014), global polysome traces were similar in the wild-type and *puf3Δ* cells grown in the fermentable medium, indicating no obvious overall translation defects by deletion of Puf3p (Supplemental Figure S2A). For northern analysis, RNAs in the sucrose gradient fractions were isopropanol-precipitated and were subjected to formaldehyde-agarose gel electrophoresis. Although the amount of total RNAs in each fraction varied depending on the fractionated position, the overall distributions of total RNAs in the wild type and *puf3Δ* resembled each other (Supplemental Figure S2B).

We selected the following total four types of mRNAs for further analyses; polysome-enriched mRNAs that do not encode mitochondrial proteins (*type 1*), polysome-enriched mRNAs encoding nc-mitochondrial proteins (*type 2*), and monosome-enriched nc-mitochondrial mRNAs *(type 3* and *type 4*). The monosome-enriched nc-mitochondrial mRNAs were further classified by the Puf3p sites to focus on translational regulation of Puf3p to these mRNAs; monosome-enriched nc-mitochondrial mRNAs with the Puf3p binding sequence (*type 3*), or without the Puf3p binding sequence (*type 4*). As described previously (Heyer and Moore 2016), many monosome-enriched mRNAs show lower expressions than other mRNAs upon fermentable media. We confirmed this expression tendency of monosome-enriched nc-mitochondrial mRNAs by RT-PCR or northern blotting. Due to the technical difficulty for further analysis, mRNAs with relatively higher abundances upon fermentable media were selected. According to the above criteria, we finally

picked mRNAs; *ACT1*, *ILV5*, a pair of *MRPL16* and *RSM10*, and a pair of *AIM17* and *CAT5/COQ7* as representatives of *type 1–type 4* mRNAs, respectively (Supplemental Table S1).

In the wild-type cells, more than 75% of *ACT1* mRNA (*type 1*), one of the constitutively translated non-mitochondrial mRNAs, was clearly translated in heavy polysomes (more than 3 ribosomes; fractions 9–13 in Figure 1A, 1D and 1F). Average mRNA occupancies in the polysomes (light and heavy) were 94.6% (Figure 1F). Likewise, 64.5% of *ILV5* (*type 2*; polysome-enriched nc-mitochondrial mRNA) was mainly translated in the heavy polysomes, and showed a quite similar mRNA distribution pattern to that of *ACT1* (Figure 1A). Consistent with the ribosome footprinting analysis of *ILV5* mRNA using the dataset of Heyer and Moore (2016) (Supplemental Figure S1B), mRNA population of *ILV5* in the small-number ribosome fractions (monosomes and light polysomes) was much higher than that of *ACT1* (Figure 1F). In contrast, monosome-enriched nc-mitochondrial mRNAs (*type 3* and *type 4*), *MRPL16*, *RSM10*, and *CAT5/COQ7*, were apparently translated in the small-number ribosome fractions (Figure 1B, 1C, and 1E). Northern analyses showed that these *type 3* and *type 4* mRNAs still have the highest mRNA population in the polysomes, while approximately 40% of their total mRNAs were translated in the light polysomes, which resulted in relative flat distributions of the mRNAs from monosomes to heavy polysomes in the wild-type cells (Figure 1B, 1C, 1E and 1F). A partial exception for the *type 3* and *type 4*, *AIM17* mRNA (*type 4*) distributed similarly to *ILV5* (*type 2*; Figure 1D and 1F). Given that *AIM17* mRNA has a longer ORF length (1,398 nt) than the other *type 3* and *type 4* mRNAs analyzed here (612–702 nt) and that the length is relatively similar to that of *ILV5* mRNA (1,188 nt), it may simply reflect the loading capacity of ribosomes depending on the ORF length, leading the different mRNA distribution of *AIM17*.

Many monosome-enriched nc-mitochondrial mRNAs are localized on the mitochondrial surface on a Puf3p dependent or independent manner (Supplemental Table S1). *MRPL16* and *RSM10* (*type 3*), *AIM17* and *CAT5* (*type 4*) are all localized on the mitochondrial outer membrane, although the polysome-enriched *ILV5* (*type 2*) is not the case (Saint-Georges et al. 2008). Curiously,

the deletion of Puf3p decreases the proportion of those localized mRNAs; *MRPL16*, *RSM10*, *AIM17* and *CAT5*, but inversely induces the mRNA localization of *ILV5* (Saint-Georges et al. 2008). Here, our polysome analysis revealed that the absence of Puf3p did not change significantly the mRNA distributions of *ACT1* and *ILV5* (*type 1* and *type 2*), which are mainly translated in heavy polysomes, and rather slightly increased the number of ribosomes per mRNA in these two mRNAs (Figure 1A). This is also apparent when sucrose density gradient fractions were divided into four bins, namely, non-ribosomal cytosol, monosomes, light polysomes, and heavy polysomes, to allow more quantitative comparison (Figure 1F). On the contrary, *MRPL16* (*type 3*), *AIM17* and *CAT5* (*type 4*) mRNAs were mildly shifted to the monosomes; the peak in the heavy polysomes fell in the absence of Puf3p (Figure 1B, 1D, 1E and 1F). Another *type 3* mRNA, *RSM10*, was also altered its distribution pattern in the *puf3Δ* (Figure 1C), while the difference is not so noticeable as other *type 3* and *type 4* mRNAs (Figure 1F). Thus, Puf3p certainly impacted on translations of the monosome-enriched mRNAs of both *type 3* and *type 4* rather than the polysome-enriched ones. These effects were partially different depending on the transcripts. Given that Puf3p has influence on mRNA translations in a broader range beyond its canonical targets (Freeberg et al. 2013; Kershaw et al. 2015; Lapointe et al. 2018), that might include some indirect effects by Puf3p.

Deletion of Puf3p marginally affects the abundance of mRNAs, even those lacking the canonical Puf3p target sequence.

Previous studies revealed that Puf3p controls mRNAs decay, which is involved in mitochondrial functions, in transcript-specific and carbon source-dependent manners (Jackson et al. 2004; Miller et al. 2014; Olivas and Parker 2000). We then verified expression of monosome-enriched mRNAs in the presence or absence of Puf3p (Figure 2; see also Supplemental Figure S3 for the total RNA migration pattern). Northern blot analyses were conducted using total RNA prepared from logarithmically growing yeasts. Relative abundance of the polysome-enriched *ILV5* mRNA (*type 2*)

was similar between the wild-type and *puf3Δ* yeasts grown in the fermentable medium. The average alteration of relative *ILV5* mRNA abundance (*puf3Δ*/wild type, Δ/W) was 0.92 (Figure 2A). In contrast, those for the *type 3* mRNAs, *RSM10* and *MRPL16*, slightly increased in the cells lacking Puf3p (Δ/W, 1.31 for *RSM10* and 1.37 for *MRPL16*; Figure 2A), implying that Puf3p promotes mRNA decay slightly in the carbon-source dependent manner (Jackson et al. 2004; Miller et al. 2014; Olivas and Parker 2000). Actually, in the case of *RSM10*, it was reported that Puf3p does not affect the mRNA level (Miller et al. 2014), while our analysis reproducibly showed loss of Puf3p slightly enhanced the expression of *RSM10* mRNA. Because *S. cerevisiae* genetic variability leads to different phenotypes related to mitochondria (Montanari et al. 2014), this expression variance of *RSM10* mRNA may be caused by difference in genetic backgrounds.

The other type of monosome-enriched nc-mitochondrial mRNAs (*type 4*) showed transcript-dependent expression patterns; *AIM17* mRNA was de-stabilized in the *puf3Δ* mutant (W/Δ=0.74) whereas *CAT5* mRNA was expressed slightly more (W/Δ=1.22; Figure 2A). Both mRNAs lack the canonical Puf3p binding sequence. However, Puf3p fine-tuned these mRNA levels. In line with the indirect moderation by Puf3p, non-mitochondrial mRNA, *ACT1* (*type 1*), was also altered its mRNA abundance by loss of Puf3p (Figure 2A).

To further verify if Puf3p regulates mRNA abundance of monosome-enriched mRNAs in a carbon source dependent manner, we performed the northern analysis using total RNAs prepared from yeasts grown in respiratory media (YPGal or YPGly). As shown in Figure 2B, steady-state mRNA levels of two types of monosome-enriched mRNAs, *MRPL16* (*type 3*) and *CAT5* (*type 4*), were not strongly affected by the *puf3Δ* mutation in YPGal or YPGly. The relative changes of the mRNAs (w/Δ) were lower than those in YPD in both mRNAs (Figure 2A and 2B), suggesting that Puf3p slightly modulates mRNA abundance of monosome-enriched mRNAs in a transcript-specific manner especially under the glucose-rich media.

Puf3p works as a translational repressor of Mrpl16p and Cat5p in a carbon source-dependent manner.

Besides roles on mRNA decay, Puf3p is well considered as a spatial repressor for translation of nc-mitochondrial mRNAs until they reach the vicinity of mitochondria (Crawford and Pavitt 2019). In the case of *COX17* mRNA, however, *puf3Δ* does not affect the Cox17p level even though Puf3p promotes degradation of *COX17* mRNA (Olivas and Parker 2000), implying intricate roles of Puf3p on its targets. To clarify impacts of Puf3p on the translation of the monosome-enriched nc-mitochondrial mRNAs (*type 3* and *type 4*), we analyzed endogenous levels of Mrpl16p and Cat5p via western blotting.

As shown in Figure 3A, a steady-state level of Mrpl16p in the wild-type strain was very low in the fermentable medium (YPD). Reflecting the mitochondrial activity, however, relative abundance of Mrpl16p drastically increased by approximately 8–9 times in the respiratory media (YPGal or YPGly; Figure 3B). Similarly, another mitochondrial protein, Cat5p, displayed the high induction under these growth conditions, akin to Mrpl16p (Figure 3D). The wild-type cells expressed Cap5p in the fermentable medium approximately 3–4 times lower than in the respiratory media and remarkably increased protein synthesis in response to the mitochondrial activity (Figure 3E). Importantly, deletion of Puf3p enhanced both Mrpl16p and Cat5p levels in the fermentable medium while the effect was less significant than in the respiratory media (Figure 3A, 3B, 3D, and 3E). In the respiratory media, Puf3p still worked as the translational repressor for Cat5p, whereas Puf3p did not repress translation of Mrpl16p (Figure 3A, 3B, 3D, and 3E). The effects of Puf3p-driven translation inhibition were somehow different between Mrpl16p and Cat5p. Above results indicate that Puf3p acts as a negative regulator of monosome-enriched mRNAs at the post-transcriptional level in a carbon source- and/or transcript-dependent manner.

Of note, given that *CAT5* mRNA lacks the canonical Pup3p binding sequence and none of the previous studies identified *CAT5* as a bona fide Puf3p target so far, it was a quite surprise that

Cat5p expression is clearly repressed by Puf3p in all carbon sources (Figure 3D–3F). *CAT5* encodes Cat5p/Coq7p involved in the CoQ biosynthetic pathway (Jonassen et al. 1998; Marbois and Clarke 1996). Recent multi-omics analyses revealed that yeast Puf3p directly regulates the CoQ biosynthesis especially via Coq5p (Lapointe et al. 2018). Coq5p catalyzes the *C*-methylation ring modification step prior to the hydroxylation step via Cat5p (Awad et al. 2018). The multi-omics analyses pointed out that yeast strains lacking Puf3p are significantly deficient for CoQ under the fermentation, but not under the respiration (Lapointe et al. 2018). Further, they first picked up *CAT5* as a candidate for the Puf3p target in the CoQ biosynthesis pathway including other six COQ genes. According to the integration of HITS-CLIP and RNA Tagging data, however, they eventually excluded *CAT5* from high-confidence Puf3p targets (Lapointe et al. 2018). As mentioned earlier, Puf3p broadly impacts on translation beyond its classical targets (Freeberg et al. 2013; Kershaw et al. 2015; Lapointe et al. 2018). Therefore, *CAT5* mRNA translation would be regulated by Puf3p as one of the relevant CoQ pathway products directly or indirectly in a way different from *MRPL16* mRNA.

Puf3p binds non-canonical sequences that have a variation at the 7th position of the canonical sequence on *MRPL16* and *CAT5* mRNAs *in vitro*.

As presented in Figures 1–3, our analysis uncovered that Puf3p controls the translation of the *CAT5* mRNA and partially its expression *in vivo*. As shown in Figure 4A, three amino acid residues within each Puf repeat, which directly contact with a single base of RNA and determine binding specificity dominantly (Zhu et al. 2009; Cheong and Hall 2006; Opperman et al. 2005; Miller et al. 2008; Wang et al. 2009; Varshney et al. 1991; Koh et al. 2009). *CAT5* mRNA does not have any canonical Puf3p binding sequence, UGUANAUA. In contrast, there is one similar sequence, UGUAUAAA, which has one difference at the 7th nucleotide of the Puf3p binding sequence (A instead of U), in the 92–99 nt positions of the *CAT5* 3'-UTR (Figure 4C).

To directly evaluate if *CAT5* mRNA is a bona fide target of Puf3p, we employed an *in vitro* binding assay between Puf3p and the 3'-UTRs of *MRPL16* and *CAT5* mRNAs according to the previous analyses (Houshmandi and Olivas 2005; Jackson et al. 2004). We purified the glutathione *S*-transferase-tagged Puf3p repeat domain (Puf3-RD; 465–879 amino acids) expressed in *E. coli*, and *in vitro*-transcribed RNAs corresponding to the 3'-UTRs of *MRPL16* and *CAT5* mRNAs with or without mutations were labeled with Cy3. These materials were subjected to the electrophoretic mobility shift assay (EMSA). Increasing concentrations of purified recombinant Puf3-RD (0–1.95 μM) were incubated with a fixed amount of labeled wild-type or mutated RNAs (Figure 4D and 4E).

As shown in Figure 4D, Puf3p bound the wild-type *MRPL16* 3'-UTR dose-dependently, yielding the gradual appearance of a shifted band when increasing Puf3-RD was used in EMSA (lanes 1–3). This binding occurred through Puf3p but not simply through the GST tag, as there was no bind shift in the presence of GST protein alone (G; lane 4). Strikingly, the *mrpl16-101*, in which the first 4 nucleotides of the canonical sequence, UGUA, were replaced with ACAC, still showed the clear band shift depending on the amount of Puf3-RD (Figure 4D, lanes 5–7). According to Lee and Tu (Lee and Tu 2015), the UGUA substitution of Puf3p targets is sufficient to abolish the binding affinity with Puf3p. Nevertheless, the *mrpl16-101* 3'-UTR with this substitution retained the binding affinity with Puf3-RD. We then searched an additional Puf3p binding sequence within the 64 nt of the *MRPL16* 3'-UTR (Nagalakshmi et al. 2008). There is one sequence similar to the Puf3p binding sequence, UGUAUACA, an 8-nt with a U to C substitution at the 7th position, right before the canonical Puf3p binding sequence. We generated an *mrpl16-102* mutant, which has additional substitutions UGUA to ACAC in a candidate for the Puf3p binding sequence applied to *mrpl16-101*, and then performed EMSA (Figure 4B). The *mrpl16-102* 3'-UTR showed no band shifts irrespective of the presence of Puf3-RD, and all the mutant RNA remained as the lower free RNA band (Figure 4D, lanes 9–11). Thus, these *in vitro* results indicated that *MRPL16* mRNA has two distinct Puf3p binding sites; the canonical one and a variant with one nucleotide substitution at the 7th position of the canonical sequence.

Next, we prepared the 115 nt of the *CAT5* mRNA 3'-UTR as a wild-type substrate and conducted EMSA as shown in Figure 4E. EMSA clearly showed that the wild-type *CAT5* 3'-UTR directly interacted with Puf3-RD (Figure 4E, lanes 2 and 3). The shifted band corresponding to the RNA-protein complex appeared in the presence of Puf3-RD but not in its absence, or in the presence of GST alone (Figure 4E, lanes 1 and 4). Inversely, the lowest band corresponding to the free *CAT5* 3'-UTR disappeared when Puf3-RD was incubated with the wild-type *CAT5* 3'-UTR, likewise *MRPL16* (Figure 4E, lanes 2 and 3). Then, we tested if a mutated version of *CAT5* mRNA, *cat5-101*, which has the UGUA to ACAC mutation in the candidate of the non-canonical Puf3p binding sequence (Figure 4C), binds to Puf3-RD *in vitro*. As expected, the *cat5-101* 3'-UTR completely lost the binding ability with Puf3-RD, and there was no reduction of the free RNAs regardless of the presence or absence of Puf3-RD (Figure 4E, lanes 5–8). An additional band (*) was observed when the *CAT5* or *cat5-101* 3'-UTRs were present (lanes 1–8), however, this was nonspecific because it was observed independent of the presence or absence of Puf3-RD or GST. Overall, we concluded that *CAT5* mRNA is a novel bona fide Puf3p target displaying the physical interaction with Puf3p via the non-canonical Puf3p binding sequence UGUAUAAA *in vitro*.

From the above *in vitro* analysis of *MRPL16* and *CAT5* 3'-UTRs, Puf3p was revealed to accept U to C and U to A variants of the 7th position on the canonical 8-nt binding sequence. Thus, it is possible that Puf3p recognizes wider mRNAs *in vivo* than the strict targets identified by previous reports (Freeberg et al. 2013; Kershaw et al. 2015; Lapointe et al. 2018). In addition, some of mRNAs may have multiple canonical and/or non-canonical Puf3p-binding sites with redundant functions.

The non-canonical Puf3p binding sequence of *CAT5* mRNA is required for proper expression of Cat5p under the fermentation as well as the respiration conditions.

To clarify whether the novel Puf3p binding sequence of *CAT5* mRNA found in the *in vitro* analyses has functions *in vivo*, we generated a mutant strain with the UGUA to ACAC mutation in the above mentioned non-canonical Puf3p binding sequence of the *CAT5* gene (*cat5-101*). As shown in Figure 5A, the *cat5-101* strain grew normally like the wild-type cells both on the fermentable and the respiratory media (YPD and YPGly) at 30˚C and 37˚C (Supplemental Figure S4A). In contrast, *cat5* deletion strains (*cat5Δ* or *cat5Δpuf3Δ*) grew on YPD but not on YPGly at 30˚C or at 37˚C (Figure 5A and Supplemental Figure S4A), consistent with the respiratory-deficient phenotypes reported previously (Tran et al. 2006). Since Puf3p mainly regulated Cat5p levels in a post-transcriptional manner (Figure 3D–3F), we thought that the Puf3p binding affinity to *CAT5* mRNA may affect translation of Cat5p. Western blot analysis showed that the *cat5-101* strain has less amount of Cap5p than the wild type in YPD medium (Figure 5B, lanes 1 and 2). Importantly, the level of Cat5p produced in the *cat5-101* mutant was similar regardless of the presence or absence of Puf3p (Figure 5B, lanes 2 and 5). Considering that the *puf3Δ* clearly enhanced the Cat5p expression level (Figure 3D–3F; Figure 5B, lane 4), the decreased Cap5p levels in the *cat5-101* mutant may be caused by another protein binding to this non-canonical binding sequence, UGUAUAAA, rather than the deficient Puf3p binding. The similar phenotype regarding Cat5p expression pattern was also observed in the *cat5-101* cells grown in YPGly (Figure 5C). Under the respiratory conditions, the *cat5-101* mutation reduced the Cat5p level more strongly regardless of the presence or absence of Puf3p (Figure 5C, lanes 2 and 4). Thus, Puf3p binding on the non-canonical Puf3p binding site in the *CAT5* 3'-UTR is not required for yeast growth in the respiratory medium, but clearly contributes to upregulation of Cat5p translation under respiration. Moreover, the non-canonical Puf3p binding site seems to recruit an unidentified factor(s) that enhances Cat5p production under the fermentable and respiratory conditions to cooperate with Puf3p in *CAT5* post-transcriptional regulation.

In this study, we uncovered that Puf3p directly interacts with the non-canonical Puf3p binding sequences with variation at the 7th position *in vitro* and *in vivo* (Figures 4 and 5). The N-

terminal part of a PUF domain, which recognizes the 3' region of the Puf3p site, seems to be more flexible for accepting target-nucleotide mutations than the C-terminal part (Campbell et al. 2014; Zhou et al. 2021). Indeed, analysis of human PUM2 binding sites using SEQRS *in vitro* and PAR-CLIP *in vivo* revealed that substitutions of the 7th position of the canonical sequence to A or C are naturally occurred (Campbell et al. 2012, 2014). Alternatively, several PUF proteins show broader specificity through ejection of certain undesirable nucleotides (Gupta et al. 2008; Wang et al. 2009). We don't know yet how Puf3p-RD structurally recognizes the variant sequences with possessing the altered 7th position, but as proposed by Zhou *et al*. (Zhou et al. 2021), an equilibrium between individual binding specificity of each repeat to the corresponding nucleotide and total binding affinity to the target mRNAs in PUF proteins may be crucial. In fact, consistent with the previous structural study (Campbell et al. 2014), their three-hybrid analysis also confirmed that the N-terminal part of the PUF domain is more tolerable for combinatorial mutations of the target nucleotides than the C-terminal part (Zhou et al. 2021).

Further, the *cat5*-mutant analysis revealed that *CAT5* mRNA, one of those mRNAs regulated by Puf3p via the non-canonical Puf3p binding sequence, is regulated not only by Puf3p but also by another protein(s) *in vivo* (Figure 5B and 5C). Puf3p predominantly represses *CAT5* expression in the fermentable medium compared to the respiratory one while the mutation of *CAT5*'s non-canonical Puf3p site leads to reduction of Cat5p production (Figures 2, 3D–F, and 5B–C). Therefore, this non-canonical Puf3p binding site is recognized by multiple factors including Puf3p, and their binding may be controlled through environmental carbon sources. Although Puf4p and Puf5p, other Pumillio family proteins in the yeast, which partially share target mRNAs with Puf3p (Gerber et al. 2004; Lapointe et al. 2017) are candidates of this unknown factor(s), their known-targets differ from the non-canonical Puf3p-biding sequence of *CAT5* mRNA. In either case, Puf3p and the other factor(s) need to be controlled in a carbon-source dependent manner. Puf3p activity is, at least, regulated via phosphorylation depending on the carbon sources (Bhondeley and Liu 2020; Lee et al. 2015). Moreover, according to the polysome analysis (Figure 1), significant

portions of certain nc-mitochondrial mRNAs (*type 3* and *type 4*: in particular *MRPL16*) were associated with the monosome in the absence of Puf3p. Because the *puf3Δ* upregulates stabilities and/or translation of such mRNAs, these mRNAs in the monosome fractions may positively contribute to production of the mitochondrial proteins, and Puf3p might somehow inactivate translation through suppressing enrichment of the mRNAs in the monosome fractions. It is also possible that phosphorylation of Puf3p might affect such activity, and that Puf3p-driven regulation on the translational level allows more rapid response of mitochondrial biogenesis to fluctuation in glucose availability than transcriptional regulation (Molenaar et al. 2009). This kind of translational regulation may be active in higher eukaryotes. A human homologue of *CAT5*/*COQ7* rescues yeast CoQ_6 deficiency caused by *cat5Δ* mutation (Awad et al. 2018; Vajo et al. 1999), and the 3'-UTR of human *CAT5* (*hCOQ7*) mRNA can recruit human Pumillio proteins PUM1 and PUM2 (Bohn et al. 2018).

Further analyses are required for full understanding of Puf3p-driven translational regulation. How wide is a range of non-canonical RNA sequences recognized by Puf3p? What is the mechanism of translational regulation of Puf3p related to monosome-polysome balancing? How does Puf3p phosphorylation alter this translational repression? What is the unknown factor(s) and its/their function(s)? The understanding of the Puf3p-driven translational regulation, especially that for *CAT5* mRNA, in the yeast will also contribute to pathological studies of the CoQ_{10} deficiency in human.

MATERIALS AND METHODS

Yeast strains, plasmids and culture conditions

Standard yeast genetic techniques and other molecular biological techniques were applied (Guthrie and Fink 1991; Green and Sambrook, 2012). *S. cerevisiae* strains used in this study are listed in Table S2. Primers and plasmids are summarized in Supplemental Tables S3 and S4, respectively. For generating a *cat5Δpuf3Δ* strain (SHSC0090), an amplified *puf3Δ::CgHIS3* fragment was introduced into a *cat5Δ* strain (SHSC0060). To make a *cat5-101* strain (SHSC0279), integration of a mutant *CAT5* 3'-UTR allele was performed using the two-step gene replacement strategy. First, the *URA3* marker was integrated at the corresponding transcribed region of the *CAT5* gene, generating a *cat5Δ::URA3* strain (SHSC0268). Subsequently, a 1.08 kb *Eco*RV–*Hind*III fragment containing the *CAT5* 3'-UTR mutant allele from pSHSC009 was integrated into SHSC0268 to replace the *URA3* marker. 5-FOA resistant clones were isolated, and correct integration was confirmed by sequencing. For generating a *cat5-101 puf3Δ* strain (SHSC0286), an amplified *puf3Δ::CgHIS3* fragment was introduced into SHSC0279.

Strains were grown at 30˚C in YPD [1.0%(w/v) yeast extract, 2.0%(w/v) polypeptone, and 2.0%(w/v) D-glucose], YPGal [1.0%(w/v) yeast extract, 2.0%(w/v) polypeptone, and 2.0%(w/v) D-galactose], or YPGly [1.0%(w/v) yeast extract, 2.0%(w/v) polypeptone, and 2.0%(w/v) glycerol]. For growth comparisons, cells were grown on SCD [0.67%(w/v) yeast nitrogen base without amino acids, 0.5%(w/v) casamino acids, vitamin assay, and 2.0%(w/v) D-glucose] or SCGly [0.67%(w/v) yeast nitrogen base without amino acids, 0.5%(w/v) casamino acids, vitamin assay, and 2.0%(w/v) glycerol] with 20 μg/ml appropriate amino acids and nucleobase supplements.

Polysome profiles and RNA extraction from sucrose gradient fractions

Yeast cells were cultured until log-phase (OD_{660} 0.5-0.6), and cycloheximide was added to the culture to a final concentration of 100 µg/ml. The cells were centrifuged at 4,500 ×*g* for 10 min at 4˚C in an R10A3 rotor (Hitachi Koki, Tokyo, Japan) and washed in 40 ml of Washing Buffer I [20 mM HEPES-KOH, pH7.4, 2.0 mM $Mg(OAc)_2$, 100 mM KOAc, 100 µg/ml cycloheximide] followed by centrifugation at 2,200 ×*g* for 10 min at 4˚C with a low-speed swing rotor. The resulting pellets were frozen in liquid N_2. The frozen cells were grinded in a mortar containing liquid N_2 to make a cell chunk into fine powder, and were resuspended in 2.0 ml of Lysis Buffer I [20 mM HEPES-KOH, pH7.4, 2.0 mM $Mg(OAc)_2$, 100 mM KOAc, 1.0 mM DTT, 1.0 mM PMSF, cOmplete Protease Inhibitor Cocktail, EDTA-free (Roche Diagnostics, Basel, Switzerland)]. The lysate was centrifuged at 2,900 ×*g* for 10 min at 4˚C with a low-speed swing rotor, and the supernatant was cleared by centrifugation at 9,200 ×*g* for 10 min at 4˚C in a microcentrifuge (Kubota Corp., Tokyo, Japan). After once more centrifugation under the same conditions, the supernatant was loaded onto a 10–50% (w/v) linear sucrose gradient and was centrifuged at 100,000 ×*g* for 2.0 h at 4˚C in a P28S2 rotor (Hitachi Koki). The fraction recovery was performed from top to bottom using Piston Gradient Fractionator (Biocomp Instruments, Fredericton, Canada) with monitoring A_{254}. For RNA extraction, sucrose gradient fractions were mixed with 1.6 volume of 8.0 M guanidine-HCl and final 54 ng/µl glycogen, and RNAs were precipitated by mixing with a 1/2 volume of 2-propanol and staying at -80˚C for overnight. The precipitated samples were centrifuged at 18,000 ×*g* for 25 min at 4˚C in a microcentrifuge. The pellets were dissolved in Formaldehyde Sample Buffer [0.84%(w/v) MOPS, 0.08%(w/v) NaOAc, 0.04%(w/v) EDTA-2Na, 7.4%(w/v) formaldehyde solution, 50%(v/v) Hi-Di formamide] after washing with 70% EtOH.

Crude RNA preparation and Northern blotting

Crude RNAs from mid log-phase yeast cells were extracted at 65˚C with the Na-acetate/sodium dodecyl sulfate (SDS) buffer [50 mM Na-acetate, pH5.2, 10 mM EDTA, 1.0%(w/v) SDS] and an equal volume of Acidic Phenol Chloroform [phenol:chloroform = 5:1, pH4.5] or Phenol, Saturated with Citrate Buffer [pH 4.5] (FUJIFILM Wako Pure Chemical, Osaka, Japan). The aqueous phase was separated by the addition of chloroform and subsequent centrifugation, resulting in RNAs were precipitated with 2-propanol, and the final pellets were resuspended in TE [10 mM Tris-HCl, pH 7.5 and 1.0 mM EDTA]. The crude RNAs or RNAs from sucrose gradient fractions were separated on a 1.2%(w/v) agarose gel with 2.2 M formaldehyde in the MOPS buffer, and transferred onto Hybond-N^+ charged nylon membranes (GE Healthcare, Chicago, Illinois, USA) by capillary transfer in 20×SSC. Hybridization with digoxigenin (DIG)-labeled antisense RNA probes was conducted in DIG Easy Hyb (Roche Diagnostics) at 68˚C. The antisense RNA probes of *ACT1*, *ILV5*, *AIM17*, *MRPL16*, *RSM10*, and *CAT5/COQ7* were labeled with digoxigenin using DIG Northern Starter Kit (Roche Diagnostics).

Total protein extraction and Western blotting

Mid log-phase yeast cells (0.5 OD_{600} unit) were collected by centrifugation, resuspended in 113 µl Lysis Buffer II [10 mM Tris-HCl, 1 mM EDTA-Na, 278 mM NaOH, 6.2%(v/v) β-mercaptoethanol], and incubated for 5 min on ice. Cell lysate was treated with 1.0 ml of ice-cold 10%(w/v) TCA for 10 min on ice, and centrifugated at 18,000 ×*g* for 5 min at 4˚C in a microcentrifuge. After washing with ice-cold acetone, the final pellets were resuspended in SDS-PAGE Sample Buffer [50 mM Tris-HCl, pH 6.8, 5.0 mM EDTA-Na, pH8.0, 2.5%(w/v) SDS, 12.5%(w/v) glycerol, 0.005%(w/v) bromophenol blue, 2.0%(v/v) β-mercaptoethanol, 2.0 mM PMSF] supplemented with final 20 mM Tris, and heated for 5 min at 95˚C. Immunoblots were developed using ECL with horseradish peroxidase-conjugated goat anti-rabbit IgG as the secondary antibody. For ECL detection,

membranes were incubated for 1 min in ECL solution [100 mM Tris-HCl, pH 8.6, 0.2 mM *p*-coumaric acid in DMSO, 1.2 mM luminol sodium salt in DMSO, 0.01%(w/v) H_2O_2] (Raue et al. 2007). Antibodies against Mrpl16p and Cat5p/Coq7p was kindly provided by Prof. Antonio Barrientos (University of Miami, USA) and Prof. Catherine F. Clarke (UCLA, USA), respectively.

Protein expression and purification

The GST-Puf3RD expression plasmid, pTYE600, and its vector, pGEX-4T-2, were introduced into the *Escherichia coli* strains BL-21 (DE3) or TG1 [*supE hsdΔ*5, *thi*, Δ(*lac-proAB*)/F' [*traD*36, *proAB*$^+$, *lacI*^{q}, *lacZΔ*M15]. GST-tagged fusion proteins were overexpressed by inducing cultures in log phase with 0.2 mM IPTG at 37˚C for 2 h. Collected cells were washed with ice-cold STE Buffer [10 mM Tris-HCl, pH 8.0, 0.1 M NaCl, 1 mM EDTA-Na], and resuspended with ice-cold Lysis Buffer III [50 mM Tris-HCl, pH 7.5, 100 mM NaCl, 2 mM EDTA-Na, 1 mM PMSF]. Cells disruption was performed with Ultrasonic Disruptor UD-201 (Tomy, Tokyo, Japan). In advance of centrifugation for removing cells debris, the cell lysate was incubated with 0.1%(w/v) Trition X-100 on ice for 5 min. The GST fusion proteins were purified with Glutathione Sepharose ™4B (GE Healthcare) according to the manufacturer's protocol with Binding Buffer I [50 mM Tris-HCl, pH 7.5, 0.1%(w/v) Triton X-100, 2 mM EDTA-Na, pH8.0, 0.1 M NaCl, 1mM PMSF] and Elution Buffer [50 mM Tris-HCl, pH 8.0, 25 mM reduced glutathione]. Protein eluates were dialyzed against 50 mM Tris-HCl, pH 8.0, and protein concentration of the final samples were determined by the Bradford assay using Protein Assay CBB Solution (Nakalai Tesque, Kyoto, Japan) and bovine serum albumin (FUJIFILM Wako Pure Chemical) as a standard.

In vitro transcription and fluorescence labeling of RNA

DNA templates were amplified from pTYE611 (*MRPL16* 3'-UTR), pTYE612 [*mrpl16* 3'-UTR w/o Puf3 site (26TGTA to 26ACAC)], pSHE002 [*mrpl16* 3'-UTR double mutations (18TGTA to 18ACAC, 26TGTA to 26ACAC)], pTYE613 (*CAT5/COQ7* 3'-UTR), or pSHE001 [*cat5/coq7* 3'-UTR (92TGTA to 92ACAC)] with MRPL16_3UTR_rv2 or CAT5_3UTR_rv2, and M13-20 as primers. The resulting PCR products were purified with illustra GFX PCR DNA & Gel Band Purification Kit (GE Healthcare) followed by 2-propanol precipitation, and the final pellets were dissolved in DEPC-treated water (DEPC-DW). *In vitro* transcription was performed using SP6 RNA polymerase with MEGAscript kit (Ambion, Austin, Texas, USA). Transcribed RNAs were subjected to phenol chloroform extraction followed by chloroform extraction and 2-propanol precipitation, and the final pellets were dissolved in 40 µl of TE, and were further desalted with NucAway™ Spin Columns (Ambion) equilibrated with TE. The RNAs were treated with final 1.8 mg/ml $NaIO_4$ at 23˚C for 60 min in the dark, resulting in oxidization of the 2', 3'-diol at the 3'-terminus of the RNAs to a 2', 3'-dialdehyde. The buffer of the $NaIO_4$-oxidized RNAs were exchanged to 0.10 M NaOAc, pH 5.2 with PD Spin Trap G-25 (GE Healthcare). The recovered RNAs were mixed with 7.0 µl of 10 mM Cy3 hydrazide (BroadPharm, San Diego, USA) and incubated at 4˚C for 4 h in the dark for dialdehyde–hydrazide conjugation. After ethanol precipitation, the final pellets were dissolved in 10 µl of DEPC-DW, and RNAs were purified by PAGE using a 7%(w/v) TBE-urea polyacrylamide gel. Elution of RNAs was performed with 750 µl of Urea-PAGE Elution Buffer (0.30 M NaOAc, pH5.2, 5.0 mM EDTA-Na, 0.10%(w/v) SDS) under light protection for overnight, and repeated with 250 µl of the same buffer for 4 h. Eluted RNAs were extracted with a 1:1 mixture of phenol/chloroform, and then with chloroform. After precipitation with 2-propanol in the presence of 12.5 µg/ml glycogen, the final pellets were dissolved in 20 µl DEPC-DW. For quantifying of fluorescence-labeled RNAs, the RNAs were separated on a 7%(w/v) TBE-urea polyacrylamide gel, and the signals were detected with a laser scanner, Typhoon FLA-7000 (GE Healthcare), or a cooled CCD camera system, Ez-Capture (ATTO, Tokyo, Japan).

Electrophoretic mobility shift assay (EMSA)

In vitro binding analysis regarding with GST-Puf3RD were basically performed as previously described (Houshmandi and Olivas 2005; Jackson et al. 2004). Reaction mixtures were prepared in 20 µl of Binding Buffer II [10 mM HEPES-KOH, pH 7.4, 50 mM KCl, 1.0 mM EDTA-Na, 2.0 mM DTT, 200 U/ml RNasin, 0.1 mg/ml bovine serum albumin, 0.01%(w/v) Tween-20, 0.1 mg/ml poly(rU), and 10 µg/ml yeast tRNA] in the presence (0.65 µM) or absence of GST-Puf3RD or GST with final 600 pM and 100 pM fluorescence-labeled *in vitro* transcripts of the *MRPL16* 3'-UTR and *CAT5* 3'-UTR, respectively. The mixtures were incubated at 24˚C for 30 min, received 5.0 µg of heparin, and incubated further at 24˚C for 10 min. For electrophoresis using 7%(w/v) TBE-acrylamide gel, the reaction mixtures were mixed with 4.0 µl of 5× Gel-shift Sample Buffer [5× TBE, 25%(w/v) sucrose]. Electrophoresis was performed at 200 V at 4˚C for 2–2.5 h. Fluorescence signals were detected with Typhoon FLA-7000 (GE Healthcare), and the data were processed by a software, Image Quant TL (GE Healthcare).

Sachiko Hayashi

ACKNOWLEDGEMANTS

We are grateful to Prof. Antonio Barrientos (University of Miami, USA) and Prof. Catherine F. Clarke (UCLA, USA) for α-Mrpl16p and α-Cat5p/Coq7p antibodies. We also thank Dr. Shintaro Iwasaki (RIKEN) for bioinformatic training and guidance. This work was supported by JSPS KAKENHI Grant number JP20K06491 to S. H, 17H05672 to T. Y., and Takeda Science Foundation.

REFERENCES

Andréasson C, Ott M, Büttner S. 2019. Mitochondria orchestrate proteostatic and metabolic stress responses. *EMBO Rep* **20**: e47865. doi:10.15252/embr.201947865

Attardi G, Schatz G. 1988. Biogenesis of mitochondria. *Annu Rev Cell Biol* **4**: 289–333. doi:10.1146/annurev.cb.04.110188.001445

Awad AM, Bradley MC, Fernández-del-Río L, Nag A, Tsui HS, Clarke CF. 2018. Coenzyme Q_{10} deficiencies: Pathways in yeast and humans. *Essays Biochem* **62**: 361–376. doi:10.1042/EBC20170106

Bernstein D, Hook B, Hajarnavis A, Opperman L, Wickens M. 2005. Binding specificity and mRNA targets of a *C. elegans* PUF protein, FBF-1. *RNA* **11**: 447–458. doi:10.1261/rna.7255805

Bhondeley M, Liu Z. 2020. Mitochondrial biogenesis is positively regulated by casein kinase I Hrr25 through phosphorylation of Puf3 in *Saccharomyces cerevisiae*. *Genetics* **215**: 463–482. doi:10.1534/genetics.120.303191

Bohn JA, Van Etten JL, Schagat TL, Bowman BM, McEachin RC, Freddolino PL, Goldstrohm AC. 2018. Identification of diverse target RNAs that are functionally regulated by human pumilio proteins. *Nucleic Acids Res* **46**: 362–386. doi:10.1093/nar/gkx1120

Campbell ZT, Bhimsaria D, Valley CT, Rodriguez-Martinez JA, Menichelli E, Williamson JR, Ansari AZ, Wickens M. 2012. Cooperativity in RNA-protein interactions: global analysis of RNA binding specificity. *Cell Rep* **1**: 570–581. doi:10.1016/j.celrep.2012.04.003

Campbell ZT, Valley CT, Wickens M. 2014. A protein-RNA specificity code enables targeted activation of an endogenous human transcript. *Nat Struct Mol Biol* **21**: 732–738. doi:10.1038/nsmb.2847

Chacinska A, Koehler CM, Milenkovic D, Lithgow T, Pfanner N. 2009. Importing mitochondrial proteins: machineries and mechanisms. *Cell* **138**: 628–644. doi:10.1016/j.cell.2009.08.005

Chatenay-Lapointe M, Shadel GS. 2011. Repression of mitochondrial translation, respiration and a metabolic cycle-regulated gene, *SLF1*, by the yeast Pumilio-family protein Puf3p. *PLoS One* **6**: e20441. doi:10.1371/journal.pone.0020441

Cheong CG, Hall TM. 2006. Engineering RNA sequence specificity of Pumilio repeats. *Proc Natl Acad Sci U S A* **103**: 13635–13639. doi:10.1073/pnas.0606294103

Crawford RA, Pavitt GD. 2019. Translational regulation in response to stress in *Saccharomyces cerevisiae*. *Yeast* **36**: 5–21. doi:10.1002/yea.3349

Edwards TA, Pyle SE, Wharton RP, Aggarwal AK. 2001. Structure of pumilio reveals similarity between RNA and peptide binding motifs. *Cell* **105**: 281–289. doi:10.1016/S0092-8674(01)00318-X

Endo T, Yamano K, Kawano S. 2011. Structural insight into the mitochondrial protein import system. *Biochim Biophys Acta - Biomembr* **1808**: 955–970. doi:10.1016/j.bbamem.2010.07.018

Foat BC, Houshmandi SS, Olivas WM, Bussemaker HJ. 2005. Profiling condition-specific, genome-wide regulationof mRNA stability in yeast. *Proc Natl Acad Sci U S A* **102**: 17675–17680. doi:10.1016/j.bbamem.2010.07.018

Freeberg MA, Han T, Moresco JJ, Kong A, Yang YC, Lu ZJ, Yates JR, Kim JK. 2013. Pervasive and dynamic protein binding sites of the mRNA transcriptome in *Saccharomyces cerevisiae*. *Genome Biol* **14**: R13. doi:10.1186/gb-2013-14-2-r13

Gancedo JM. 1998. Yeast carbon catabolite repression. *Microbiol Mol Biol Rev* **62**: 334–361. doi: 10.1128/MMBR.62.2.334-361.1998

García-Rodríguez LJ, Gay AC, Pon LA. 2007. Puf3p, a Pumilio family RNA binding protein, localizes to mitochondria and regulates mitochondrial biogenesis and motility in budding yeast. *J Cell Biol* **176**: 197–207. doi:10.1083/jcb.200606054

Garcia M, Darzacq X, Delaveau T, Jourdren L, Singer RH, Jacq C. 2007. Mitochondria-associated yeast mRNAs and the biogenesis of molecular complexes. *Mol Biol Cell* **18**: 362–368. doi:10.1091/mbc.E06-09-0827

Gerber AP, Herschlag D, Brown PO. 2004. Extensive association of functionally and cytotopically related mRNAs with Puf family RNA-binding proteins in yeast. *PLoS Biol* **2**: E79. doi:10.1371/journal.pbio.0020079

Gold VA, Chroscicki P, Bragoszewski P, Chacinska A. 2017. Visualization of cytosolic ribosomes on the surface of mitochondria by electron cryo□tomography. *EMBO Rep* **18**: 1786–1800. doi:10.15252/embr.201744261

Green MR, Sambrook, J eds. 2012. *Molecular Cloning: A Laboratory Manual, 4th ed. (3-Volume Set)* Cold Sprig Horbor Laboratory Press, Cold Spring Harbor, NY.

Gupta I, Clauder-Münster S, Klaus B, Järvelin AI, Aiyar RS, Benes V, Wilkening S, Huber W, Pelechano V, Steinmetz LM. 2014. Alternative polyadenylation diversifies post-transcriptional regulation by selective RNA-protein interactions. *Mol Syst Biol* **10**: 719. doi:10.1002/msb.135068

Gupta YK, Nair DT, Wharton RP, Aggarwal AK. 2008. Structures of human Pumilio with noncognate RNAs reveal molecular mechanisms for binding promiscuity. *Structure* **16**: 549–557. doi:10.1016/j.str.2008.01.006

Guthrie C, Fink GR. 1991. Guide to yeast genetics and molecular biology. *Methods Enzymol* **194**:1-933.

Heyer EE, Moore MJ. 2016. Redefining the translational status of 80S monosomes. *Cell* **164**: 757–769. doi:10.1016/j.cell.2016.01.003

Hogan DJ, Riordan DP, Gerber AP, Herschlag D, Brown PO. 2008. Diverse RNA-binding proteins interact with functionally related sets of RNAs, suggesting an extensive regulatory system. *PLoS Biol* **6**: 2297–2313. doi:10.1371/journal.pbio.0060255

Houshmandi SS, Olivas WM. 2005. Yeast Puf3 mutants reveal the complexity of Puf-RNA binding and identify a loop required for regulation of mRNA decay. *RNA* **11**: 1655–1666. doi:10.1261/rna.2168505

Jackson JS, Houshmandi SS, Leban FL, Olivas WM. 2004. Recruitment of the Puf3 protein to its mRNA target for regulation of mRNA decay in yeast. *RNA* **10**: 1625–1636. doi:10.1261/rna.7270204

Jonassen T, Proft M, Randez-Gil F, Schultz JR, Marbois BN, Entian KD, Clarke CF. 1998. Yeast clk-1 homologue (Coq7/Cat5) is a mitochondrial protein in coenzyme Q synthesis. *J Biol Chem* **273**: 3351–3357. doi:10.1074/jbc.273.6.3351

Kershaw CJ, Costello JL, Talavera D, Rowe W, Castelli LM, Sims PFG, Grant CM, Ashe MP, Hubbard SJ, Pavitt GD. 2015. Integrated multi-omics analyses reveal the pleiotropic nature of the control of gene expression by Puf3p. *Sci Rep* **5**: 15518. doi:10.1038/srep15518

Koh YY, Opperman L, Stumpf C, Mandan A, Keles S, Wickens M. 2009. A single *C. elegans* PUF protein binds RNA in multiple modes. *RNA* **15**: 1090–1099. doi:10.1038/srep15518

Lapointe CP, Preston MA, Wilinski D, Saunders HAJ, Campbell ZT, Wickens M. 2017. Architecture and dynamics of overlapped RNA regulatory networks. *RNA* **23**: 1636–1647. doi:10.1261/rna.062687.117

Lapointe CP, Stefely JA, Jochem A, Hutchins PD, Wilson GM, Kwiecien NW, Coon JJ, Wickens M, Pagliarini DJ. 2018. Multi-omics reveal specific targets of the RNA-Binding protein Puf3p and its orchestration of mitochondrial biogenesis. *Cell Syst* **6**: 125-135.e6. doi:10.1016/j.cels.2017.11.012

Lee D, Ohn T, Chiang Y-C, Quigley G, Yao G, Liu Y, Denis CL. 2010. PUF3 acceleration of deadenylation in vivo can operate independently of CCR4 activity, possibly involving effects on the PAB1–mRNP structure. *J Mol Biol* **399**: 562–575. doi:10.1016/j.jmb.2010.04.034

Lee C-D, Tu BP. 2015. Glucose-regulated phosphorylation of the PUF protein Puf3 regulates the translational fate of its bound mRNAs and association with RNA granules. *Cell Rep* **11**: 1638–1650. doi:10.1016/j.celrep.2015.05.014

Lesnik C, Golani-Armon A, Arava Y. 2015. Localized translation near the mitochondrial outer membrane: An update. *RNA Biol* **12**: 801–809. doi:10.1080/15476286.2015.1058686

Lill R, Mühlenhoff U. 2008. Maturation of iron-sulfur proteins in eukaryotes: Mechanisms, connected processes, and diseases. *Annu Rev Biochem* **77**: 669–700. doi:10.1146/annurev.biochem.76.052705.162653

Malina C, Larsson C, Nielsen J. 2018. Yeast mitochondria: An overview of mitochondrial biology and the potential of mitochondrial systems biology. *FEMS Yeast Res* **18**: foy040. doi:10.1093/femsyr/foy040

Marbois BN, Clarke CF. 1996. The *COQ7* gene encodes a protein in *Saccharomyces cerevisiae* necessary for ubiquinone biosynthesis. *J Biol Chem* **271**: 2995–3004. doi:10.1074/jbc.271.6.2995

Marc P, Margeot A, Devaux F, Blugeon C, Corral-Debrinski M, Jacq C. 2002. Genome-wide analysis of mRNAs targeted to yeast mitochondria. *EMBO Rep* **3**: 159–164. doi:10.1093/embo-reports/kvf025

Miller MA, Russo J, Fischer AD, Leban FAL, Olivas WM. 2014. Carbon source-dependent alteration of Puf3p activity mediates rapid changes in the stabilities of mRNAs involved in mitochondrial function. *Nucleic Acids Res* **42**: 3954–3970. doi:10.1093/nar/gkt1346

Miller MT, Higgin JJ, Hall TM. 2008. Basis of altered RNA-binding specificity by PUF proteins revealed by crystal structures of yeast Puf4p. *Nat Struct Mol Biol* **15**: 397–402. doi:10.1038/nsmb.1390

Molenaar D, van Berlo R, De Ridder D, Teusink B. 2009. Shifts in growth strategies reflect tradeoffs in cellular economics. *Mol Syst Biol* **5**: 323. doi:10.1038/msb.2009.82

Montanari A, Francisci S, Fazzi D'Orsi M, Bianchi MM. 2014. Strain-specific nuclear genetic background differentially affects mitochondria-related phenotypes in *Saccharomyces cerevisiae*. *Microbiologyopen* **3**: 288–298. doi:10.1002/mbo3.167

Nagalakshmi U, Wang Z, Waern K, Shou C, Raha D, Gerstein M, Snyder M. 2008. The T transcriptional landscape of the yeast genome defined by RNA sequencing. *Science* **320**: 1344–1349. doi:10.1126/science.1158441

Nilsson A, Nielsen J. 2016. Metabolic trade-offs in yeast are caused by F1F0-ATP synthase. *Sci Rep* **6**: 22264. doi:10.1038/srep22264

Olivas W, Parker R. 2000. The Puf3 protein is a transcript-specific regulator of mRNA degradation in yeast. *EMBO J* **19**: 6602–6611. doi:10.1093/emboj/19.23.6602

Opperman L, Hook B, DeFino M, Bernstein DS, Wickens M. 2005. A single spacer nucleotide determines the specificities of two mRNA regulatory proteins. *Nat Struct Mol Biol* **12**: 945–951. doi:10.1038/nsmb1010

Priesnitz C, Becker T. 2018. Pathways to balance mitochondrial translation and protein import. *Genes Dev* **32**: 1285–1296. doi:10.1101/gad.316547.118

Quenault T, Lithgow T, Traven A. 2011. PUF proteins: Repression, activation and mRNA localization. *Trends Cell Biol* **21**: 104–112. doi:10.1016/j.tcb.2010.09.013

Raue U, Oellerer S, Rospert S. 2007. Association of protein biogenesis factors at the yeast ribosomal tunnel exit is affected by the translational status and nascent polypeptide sequence. *J Biol Chem* **282**: 7809–7816. doi:10.1074/jbc.M611436200

Riordan DP, Herschlag D, Brown PO. 2011. Identification of RNA recognition elements in the *Saccharomyces cerevisiae* transcriptome. *Nucleic Acids Res* **39**: 1501–1509. doi:10.1093/nar/gkq920

Rowe W, Kershaw CJ, Castelli LM, Costello JL, Ashe MP, Grant CM, Sims PFG, Pavitt GD, Hubbard SJ. 2014. Puf3p induces translational repression of genes linked to oxidative stress. *Nucleic Acids Res* **42**: 1026–1041. doi:10.1093/nar/gkt948

Saint-Georges Y, Garcia M, Delaveau T, Jourdren L, Le Crom S, Lemoine S, Tanty V, Devaux F, Jacq C. 2008. Yeast mitochondrial biogenesis: A role for the PUF RNA-binding protein puf3p in mRNA localization. *PLoS One* **3**: e2293. doi:10.1371/journal.pone.0002293

Sharma AK, Pallesen LJ, Spang RJ, Walden WE. 2010. Cytosolic iron-sulfur cluster assembly (CIA) system: Factors, mechanism, and relevance to cellular iron regulation. *J Biol Chem* **285**: 26745–26751. doi:10.1074/jbc.R110.122218

Sylvestre J, Vialette S, Corral-Debrinski M, Jacq C. 2003. Long mRNAs coding for yeast mitochondrial proteins of prokaryotic origin preferentially localize to the vicinity of mitochondria. *Genome Biol* **4**: R44. doi:10.1186/gb-2003-4-7-r44

Tran UPC, Marbois B, Gin P, Gulmezian M, Jonassen T, Clarke CF. 2006. Complementation of *Saccharomyces cerevisiae coq7* mutants by mitochondrial targeting of the *Escherichia coli* UbiF polypeptide: Two functions of yeast Coq7 polypeptide in coenzyme Q biosynthesis. *J Biol Chem* **281**: 16401–16409. doi:10.1074/jbc.M513267200

Vajo Z, King LM, Jonassen T, Wilkin DJ, Ho N, Munnich A, Clarke CF, Francomano CA. 1999. Conservation of the *Caenorhabditis elegans* timing gene *clk-1* from yeast to human: a gene required for ubiquinone biosynthesis with potential implications for aging. *Mamm Genome* **10**: 1000–1004. doi:10.1007/s003359901147

van Dijken JP, Bauer J, Brambilla L, Duboc P, Francois JM, Gancedo C, Giuseppin MLF, Heijnen JJ, Hoare M, Lange HC, et al. 2000. An interlaboratory comparison of physiological and genetic properties of four *Saccharomyces cerevisiae* strains. *Enzyme Microb Technol* **26**: 706–714. doi:10.1016/S0141-0229(00)00162-9

Varshney U, Lee CP, RajBhandary UL. 1991. Direct analysis of aminoacylation levels of tRNAs *in vivo*: Application to studying recognition of *Escherichia coli* initiator tRNA mutants by glutaminyl-tRNA synthetase. *J Biol Chem* **266**: 24712–24718.

Walters R, Parker R. 2014. Is there quality control of localized mRNAs? *J Cell Biol* **204**: 863–868. doi:10.1083/jcb.201401059

Wang X, Chen XJ. 2015. A cytosolic network suppressing mitochondria-mediated proteostatic stress and cell death. *Nature* **524**: 481–484. doi:10.1038/nature14859

Wang X, Zamore PD, Hall TM. 2001. Crystal structure of a Pumilio homology domain. *Mol Cell* **7**: 855–865. doi:10.1016/S1097-2765(01)00229-5

Wang Y, Opperman L, Wickens M, Hall TM. 2009. Structural basis for specific recognition of multiple mRNA targets by a PUF regulatory protein. *Proc Natl Acad Sci U S A* **106**: 20186–20191. doi:10.1073/pnas.0812076106

Wang Z, Sun X, Wee J, Guo X, Gu Z. 2019. Novel insights into global translational regulation through Pumilio family RNA-binding protein Puf3p revealed by ribosomal profiling. *Curr Genet* **65**: 201–212. doi:10.1007/s00294-018-0862-4

Wickens M, Bernstein DS, Kimble J, Parker R. 2002. A PUF family portrait: 3′UTR regulation as a way of life. *Trends Genet* **18**: 150–157. doi:10.1016/S0168-9525(01)02616-6

Wiedemann N, Pfanner N. 2017. Mitochondrial machineries for protein import and assembly. *Annu Rev Biochem* **86**: 685–714. doi:10.1146/annurev-biochem-060815-014352

Williams CC, Jan CH, Weissman JS. 2014. Targeting and plasticity of mitochondrial proteins revealed by proximity-specific ribosome profiling. *Science* **346**: 748–751. doi:10.1126/science.1257522

Zhou W, Melamed D, Banyai G, Meyer C, Tuschl T, Wickens M, Cao J, Fields S. 2021. Expanding the binding specificity for RNA recognition by a PUF domain. *Nat Commun* **12**: 5107. doi:10.1038/s41467-021-25433-6

Zhu D, Stumpf CR, Krahn JM, Wickens M, Hall TM. 2009. A 5′ cytosine binding pocket in Puf3p specifies regulation of mitochondrial mRNAs. *Proc Natl Acad Sci U S A* **106**: 20192–20197. doi:10.1073/pnas.0812079106

FIGURE LEGENDS

Figure 1. Translational characteristics of nc-mitochondrial mRNAs under the fermentable conditions, which were demonstrated by polysome profiling

(A)–(E) Distribution of nc-mitochondrial mRNAs in the wild-type (WT) and *puf3* deletion (*puf3Δ*) yeasts upon polysome analyses. Northern blotting was performed using RNAs extracted from sucrose gradient fractions of the polysome analyses (blot images). Analyzed mRNAs are shown in the left. LS, loading sample; fractions 1–3, non-ribosomal cytosol; fractions 4–5, monosomes; fractions 6–8, light polysomes; fractions 9–13, heavy polysomes. The lower graph shows mRNA distribution among the sucrose gradient fractions in the above northern blotting. The graphs in (A) and (D) also show distribution of *ACT1* mRNA (blue dashed line) in addition to those of *ILV5* and *AIM17* mRNAs (black solid line), respectively. (F) A cumulative bar chart represents the ratio of mRNA occupancy in indicated fractions. mRNA signals of the fractions analyzed in each density gradient in (A)–(E) were combined into four bins (non-ribosomal cytosol, monosomes, light polysomes, and heavy polysomes), and expressed in percentage of the total signals in the fractionation. The numbers were means of the independent experiments (n=2 or 3).

Figure 2. Loss of Puf3p modestly stabilizes *RSM10*, *MRPL16* and *CAT5* mRNAs, while it destabilizes *AIM17* mRNA.

(A) Northern blot analysis of each mRNA classified as *type 1* to *type 4*. Total mRNAs were isolated from the wild-type (W) and *puf3Δ* (Δ) yeasts grown in the fermentable medium (YPD), and their total RNAs were subjected to the northern blotting for indicated mRNAs. Numbers represent relative expression changes of mRNA abundance. The means and standard deviations of mRNA

signals (Δ/W, *puf3Δ*/WT) were calculated from at least three biological replicates. (B) Northern blot analysis of *MRPL16* and *CAT5* mRNAs prepared from yeasts grown in respiratory media (YPGal and YPGly). The relative expression changes of mRNAs abundance were analyzed as described above.

Figure 3. Puf3p regulates expression of Mrpl16p and Cat5p in a carbon source-dependent manner.

(A) Steady-state levels of Mrpl16p in the wild-type (WT) and *puf3Δ* strains. Total cell extracts corresponding to the same amount of total protein were analyzed via immunoblotting using antibodies specific for Mrpl16p, and for Srp1p as a loading control. Because the expression levels of Mrpl16p differed significantly, short exposure (S) and long exposure (L) images of the same immunoblot are displayed. (B) A bar chart represents relative abundance of Mrpl16p quantified and normalized by abundance of Srp1p from more than three biological replicates in (A) (Student's *t*-test, **, $p < 0.01$; ns, not significant). (C) Relative changes of Mrpl16p in the *puf3Δ* cells compared with the wild-type cells under different growth conditions. The average of WT on YPD is set to 1.0 ($n \geq 4$; ****, $p < 0.0001$). (D) Steady-state levels of Cat5p in the wild-type (WT) and *puf3Δ* strains. Total cell extracts were analyzed as in (A). (E) A bar chart represents relative abundance of Cat5p quantified from at least three biological replicates in (D), and shown as in (B) (Student's *t*-test, ***, $p < 0.001$; **, $p < 0.01$; *, $p < 0.05$). (F) Relative changes of Cat5p in the *puf3Δ* cells compared with the WT cells ($n \geq 4$; *, $p < 0.05$; ***, $p < 0.001$).

Figure 4. Puf3p accepts variants at the 7th nucleotide of the Puf3p canonical binding sequence on *MRPL16* and *CAT5* mRNAs *in vitro*.

(A) Crystal structure of the Puf3p repeat domain (Puf3-RD) in complex with the 3'-UTR of *COX17* mRNA (PDB ID code: 3K4E). R1–R8 indicate the PUF repeats of Puf3-RD. Nucleotides of *COX17* mRNA (5'-UGUAUAUA-3') are highlighted in green for the 7th position of the canonical Puf3p binding sequence and in red for other positions of the canonical Puf3p binding sequence. (B) An overview of the Puf3-RD fusion used in this study. Shown numbers represent amino acid positions of Puf3p. (C) The upper scheme shows 3'-UTR sequences of *MRPL16* mRNA used in gel shift assays (EMSA). Shown numbers represent nucleotide positions in the 3'-UTR. Capital letters indicate the canonical Puf3p binding sequence (orange underline; U26–A33) or a candidate of a non-canonical Puf3p binding sequence with the different 7th nucleotide (24C; U18–A25). Green highlights the 7th nucleotide of the canonical or non-canonical Puf3p binding sequences. Red highlights mutated positions of the canonical or non-canonical Puf3p binding sequences. The lower scheme shows 3'-UTR sequences of *CAT5* mRNA used in EMSA. Shown numbers represent nucleotide positions in the 3'-UTR. Capital letters represent a candidate of a non-canonical Puf3p binding sequence (U92–A99), which has a different nucleotide at the 7th position (98A; green). Mutated positions are highlighted in red. (D) EMSA was performed with the wild-type and mutant forms of Cy3-labeled RNAs corresponding to the *MRPL16* mRNA 3'-UTRs. 600 pmol of the Cy3-labeled RNAs were used as substrates. The final concentration of GST-Puf3-RD used in the assays were 0 µM (–), 0.65 µM and 1.95 µM (black right triangle). Lane G (lanes 4, 8, and 12) represents control gel shift with 1.95 µM GST. No RNA substrates were included in lanes 13 and 14 in the presence of 1.95 µM GST-Puf3p-RD (+) or GST (G). (E) EMSA with the wild-type and mutant forms of the *CAT5* 3'-UTR. Assay conditions were similar to those in (D) except 100 pmol instead of 600 pmol of the Cy3-labeled RNAs were included.

Figure 5. A mutations on the non-canonical Puf3p binding sequence of *CAT5* mRNA impairs proper Cat5p expression *in vivo* but not cell viability.

(A) Growth comparison among wild-type, *cat5-101*, and *cat5Δ* strains in the presence or absence of the *PUF3* gene. Saturated cultures of the indicated strains were serially diluted by 10-fold as shown in the bottom, dropped onto YPD or YPGly plates, and cultured at 30˚C. (B)–(C) Western blot analysis of Cat5p in the corresponding yeast strains in (A). Cells were grown at 30˚C in YPD (B) or in YPGly (C). Srp1p was used as a loading control.

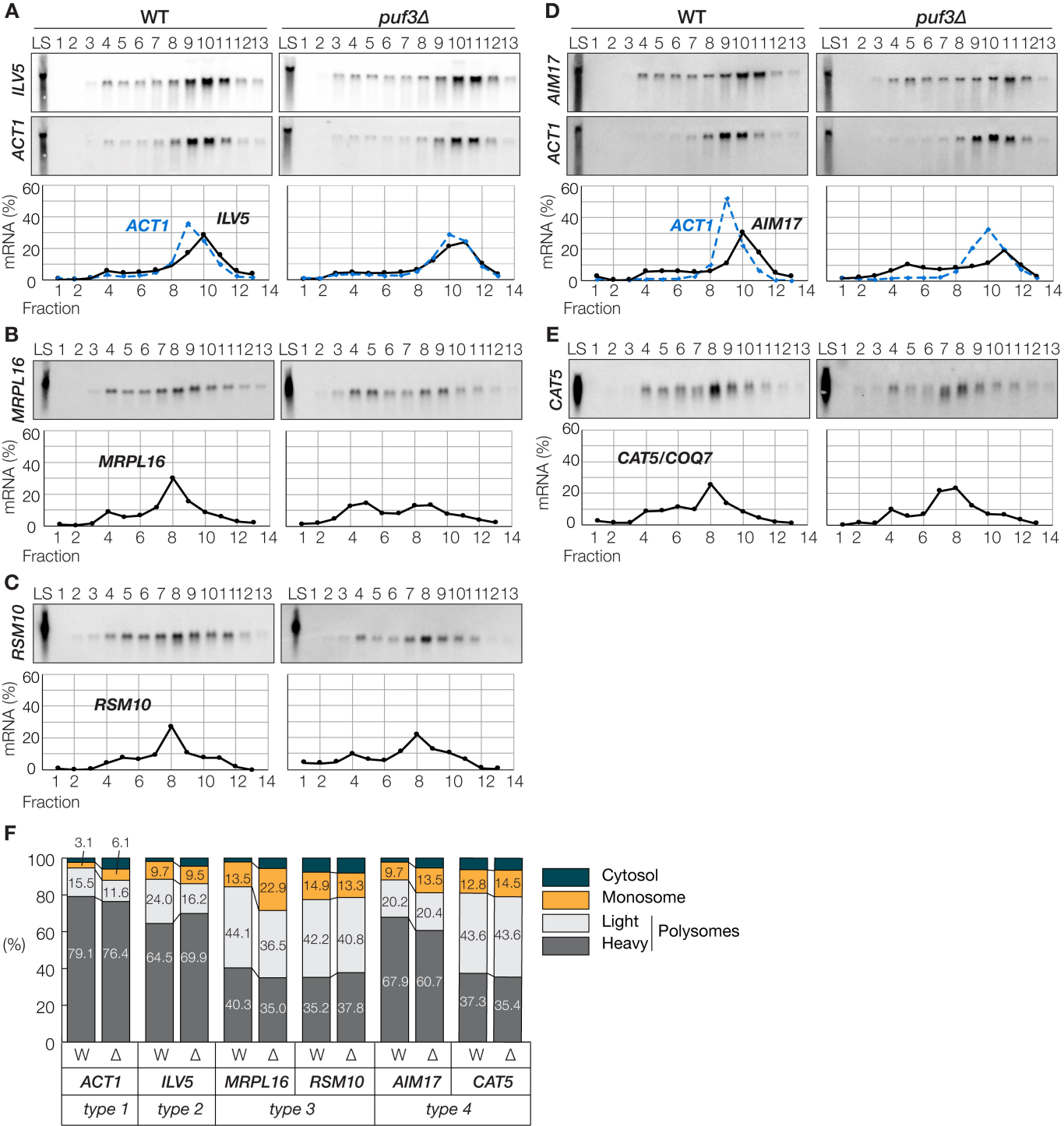
A
WT
puf3Δ
LS 1 2 3 4 5 6 7 8 9 10 11 12 13
ILV5
ACT1
mRNA (%)
ACT1
ILV5
Fraction
B
MRPL16
MRPL16
C
RSM10
RSM10
D
AIM17
ACT1
AIM17
E
CAT5
CAT5/COQ7
F
(%)
3.1
6.1
15.5
11.6
79.1
76.4
9.7
9.5
24.0
16.2
64.5
69.9
13.5
22.9
44.1
36.5
40.3
35.0
14.9
13.3
42.2
40.8
35.2
37.8
9.7
13.5
20.2
20.4
67.9
60.7
12.8
14.5
43.6
43.6
37.3
35.4
W
Δ
ACT1
ILV5
MRPL16
RSM10
AIM17
CAT5
type 1
type 2
type 3
type 4
Cytosol
Monosome
Light
Heavy
Polysomes

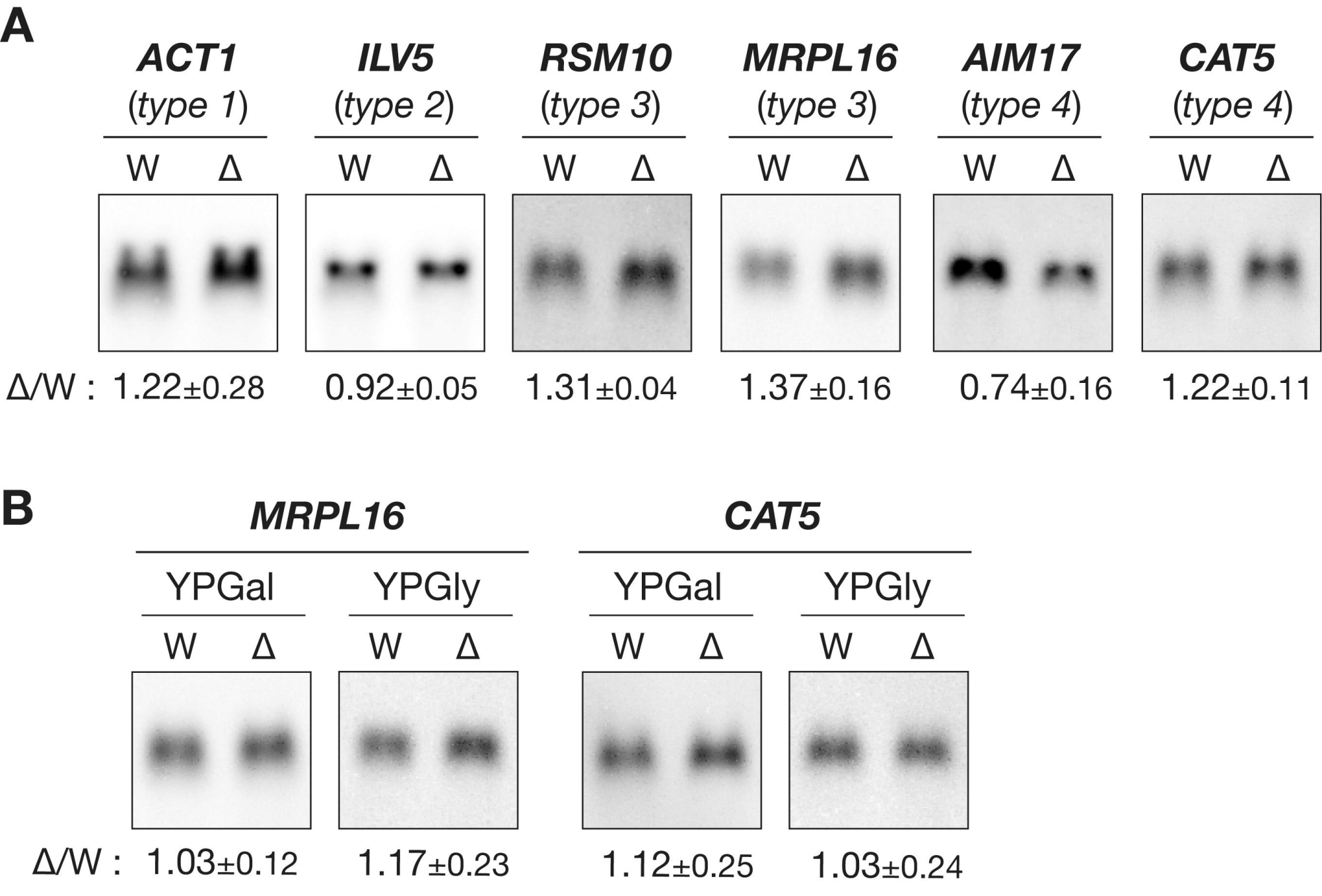
A
ACT1
(type 1)
ILV5
(type 2)
RSM10
(type 3)
MRPL16
(type 3)
AIM17
(type 4)
CAT5
(type 4)
W Δ
Δ/W : 1.22±0.28
0.92±0.05
1.31±0.04
1.37±0.16
0.74±0.16
1.22±0.11
B
MRPL16
CAT5
YPGal
YPGly
W Δ
Δ/W : 1.03±0.12
1.17±0.23
1.12±0.25
1.03±0.24

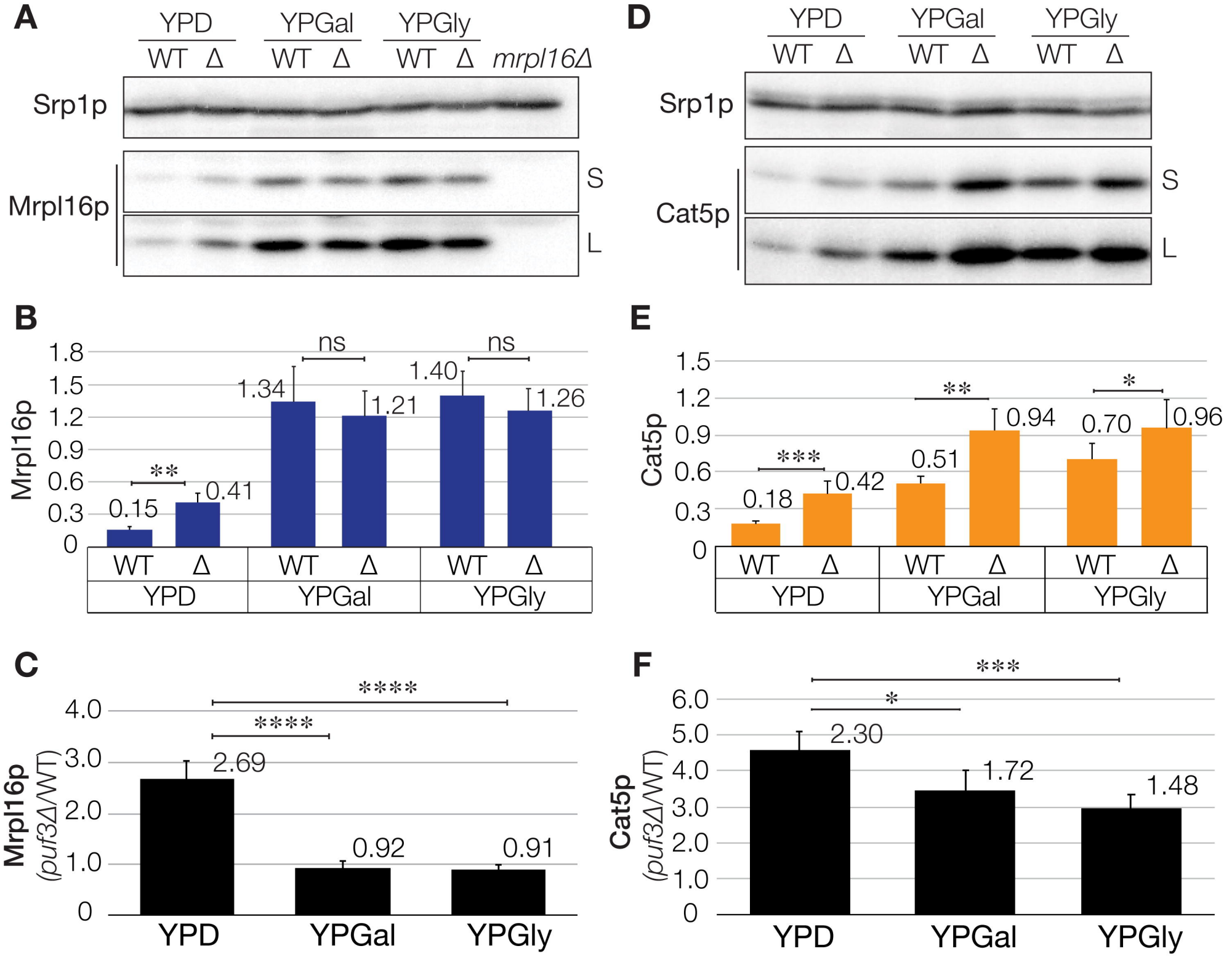
A
YPD
YPGal
YPGly
WT Δ WT Δ WT Δ mrpl16Δ
Srp1p
Mrpl16p
S
L
D
YPD
YPGal
YPGly
WT Δ WT Δ WT Δ
Srp1p
Cat5p
S
L
B
Mrpl16p
1.8
1.5
1.2
0.9
0.6
0.3
0
**
ns
ns
0.15
0.41
1.34
1.21
1.40
1.26
WT Δ WT Δ WT Δ
YPD YPGal YPGly
E
Cat5p
1.5
1.2
0.9
0.6
0.3
0
***
**
*
0.18
0.42
0.51
0.94
0.70
0.96
WT Δ WT Δ WT Δ
YPD YPGal YPGly
C
Mrpl16p
(puf3Δ/WT)
4.0
3.0
2.0
1.0
0
****
****
2.69
0.92
0.91
YPD YPGal YPGly
F
Cat5p
(puf3Δ/WT)
6.0
5.0
4.0
3.0
2.0
1.0
0
***
*
2.30
1.72
1.48
YPD YPGal YPGly

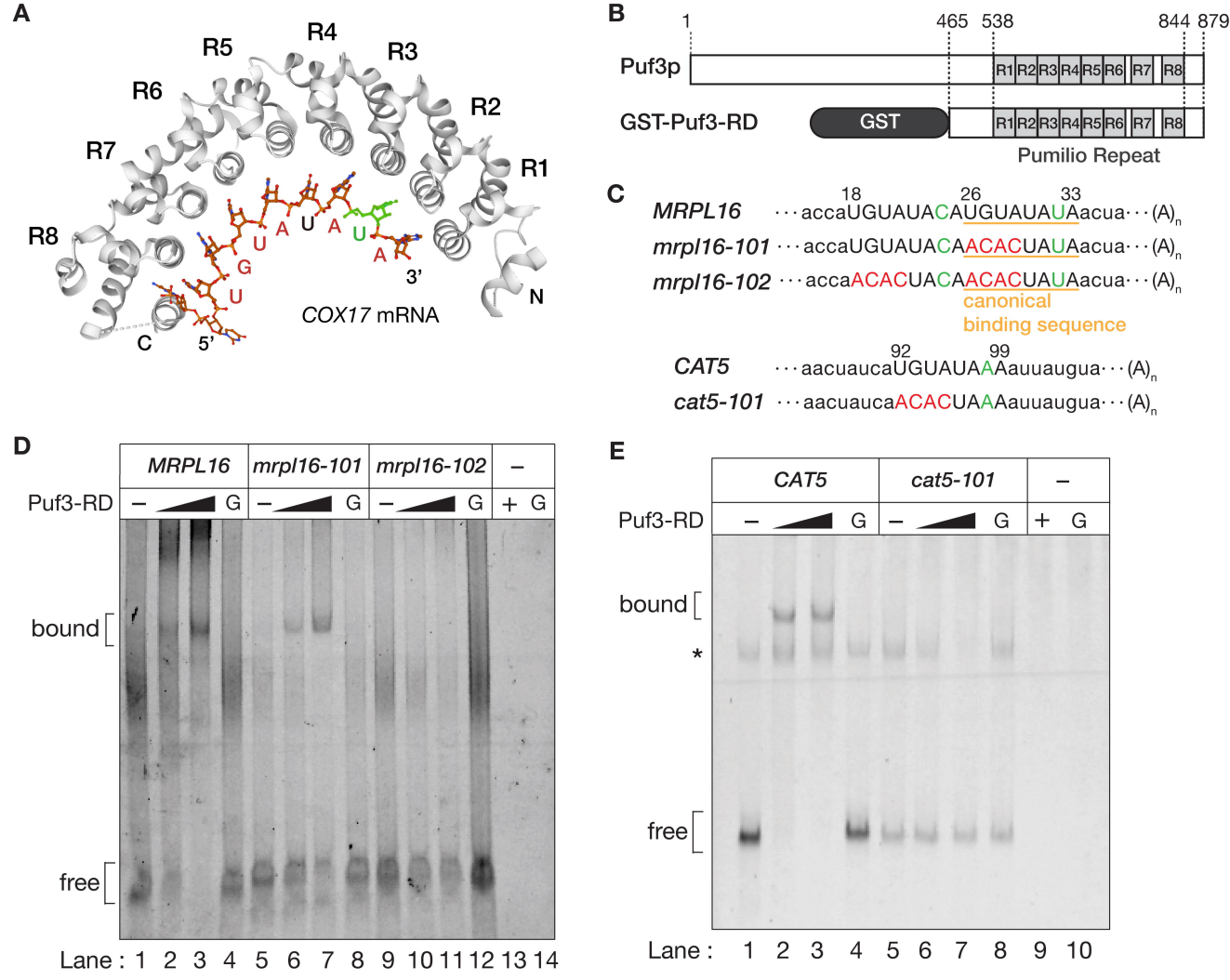
A
R5
R4
R3
R6
R2
R7
R1
R8
G
U
A
U
A
U
A
3'
N
C
5'
COX17 mRNA
B
1
465
538
844
879
Puf3p
R1 R2 R3 R4 R5 R6 R7 R8
GST-Puf3-RD
GST
R1 R2 R3 R4 R5 R6 R7 R8
Pumilio Repeat
C
18
26
33
MRPL16 ···accaUGUAUACAUGUAUAUAacua···(A)n
mrpl16-101 ···accaUGUAUACAACACUAUAacua···(A)n
mrpl16-102 ···accaACACUACAACACUAUAacua···(A)n
canonical
binding sequence
92
99
CAT5 ···aacuaucaUGUAUAAAauuaugua···(A)n
cat5-101 ···aacuaucaACACUAAAauuaugua···(A)n
D
MRPL16
mrpl16-101
mrpl16-102
–
Puf3-RD
– G
– G
– G
+ G
bound
free
Lane : 1 2 3 4 5 6 7 8 9 10 11 12 13 14
E
CAT5
cat5-101
–
Puf3-RD
– G
– G
+ G
bound
*
free
Lane : 1 2 3 4 5 6 7 8 9 10

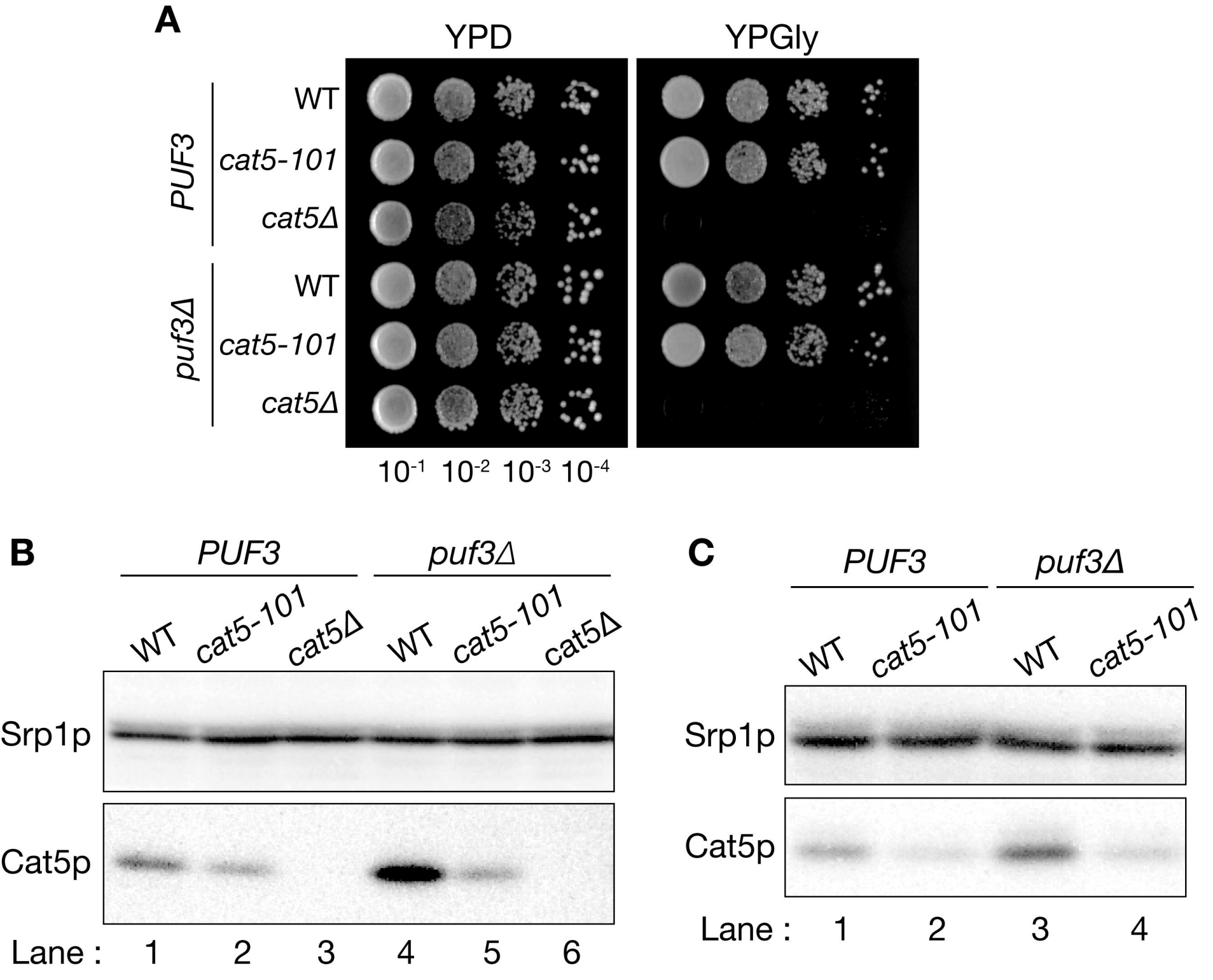
A
YPD
YPGly
PUF3
puf3Δ
WT
cat5-101
cat5Δ
WT
cat5-101
cat5Δ
10-1 10-2 10-3 10-4
B
PUF3
puf3Δ
WT
cat5-101
cat5Δ
WT
cat5-101
cat5Δ
Srp1p
Cat5p
Lane : 1 2 3 4 5 6
C
PUF3
puf3Δ
WT
cat5-101
WT
cat5-101
Srp1p
Cat5p
Lane : 1 2 3 4